Bioprinting microporous functional living materials from protein-based core-shell microgels

Yangteng Ou[1,2,3], Shixiang Cao[4], Hongjia Zhu[2], Chengzhi Guo[1], Yang Zhang[1], Wei Yan[4], Masashi Narita[5], Fengxue Xin[4], Ziyi Yu[1,*], Tuomas Knowles[2,6,*]

Author information

1 State Key Laboratory of Materials-oriented Chemical Engineering, College of Chemical Engineering, Nanjing Tech University, 30 Puzhu South Road, Nanjing, 211816, P.R. China.

2 Yusuf Hamied Department of Chemistry, University of Cambridge, Lensfield Road, Cambridge, CB2 1EW, UK.

3 Cambridge University-Nanjing Centre of Technology and Innovation, 126 Dingshan Street, Nanjing 210046, P. R. China.

4 State Key Laboratory of Materials-oriented Chemical Engineering, College of Biotechnology and Pharmaceutical Engineering, Nanjing Tech University, 30 Puzhu South Road, Nanjing, 211816, P.R. China.

5 Cancer Research UK Cambridge Institute, University of Cambridge, Cambridge, Li Ka Shing Centre, Robinson Way, Cambridge CB2 0RE, UK

6 Cavendish Laboratory, University of Cambridge, J J Thomson Avenue, Cambridge, CB3 0HE, UK

*E-mail: ziyi.yu@njtech.edu.cn; tpjk2@cam.ac.uk

Abstract

Living materials have emerged as systems bringing together material science and biology to allow the engineering and augmenting of living systems with novel functionalities. Bioprinting promises accurate control over the formation of such complex materials through programmable deposition of cells in soft materials, but current approaches had limited success on fine-tunning cell microenvironments while generating robust macroscopic morphologies. Here, we address this challenge through the use of microgel ink to bioprint functional living materials. Jammed core-shell microgels are microfluidically functionalized with cells in the aqueous cores which can promote the growth of both microbial communities and mammalian cellular spheroids, followed by an interparticle annealing to give covalently stabilized functional scaffolds with controlled microporosity that enhances the mass transfer of nutrients and metabolites. Different microbial consortia are immobilized in scaffolds towards versatile applications; more importantly, by compartmentalizing microbial consortia at microscale, the collective bioactivities of both consortia are significantly enhanced, shedding light on strategies to augment living materials with bioprocessing capabilities.

Introduction

Living materials are complex materials that incorporate living cells into non-living components[1,2]. Depending on the nature of interactions with the component cells, such materials can range from bioinert media that offer scaffolding functions[3–7], to cell-instructive biomaterials that can direct cell behaviors[8–10], and recently, even to genetically programmable matrices produced by cells that mimic the natural formation of biofilms[11–15]. The functionality of such composite materials mostly stems from embedded cells; as such, the material should always cater for cells to grow and perform properly. However, there are typically also strong constraints on the macroscopic material properties due to the functional requirement for a final structure to present a physical form that can be handled, delivered, preserved, reused, and is protective of cells. The synergy between materials and biology has not only dramatically transformed our understanding of cellular processes[16], but also brought us the capacity to engineer living systems towards a myriad of novel applications, from therapeutical delivery of cells for regenerative medicine[17–19], to on-demand production of high-value chemicals through microbial bioprocessing[6,7].

Manipulating the spatial distribution of cells is one of the most sought-after capabilities in the field of living materials. Bioprinting has arguably captured the most attention[20,21] on account of its versatility and compatibility with many cell friendly soft materials. For instance, bioprinting enables the programmable deposition of mammalian cells in bioactive hydrogels to create 3D biological constructs that better recapitulate the intricacy and heterogeneity of native tissues[22–25], which holds tremendous translational values in biomedicine. Bioprinting microbes has also seen increased applications in recent years, as it furthers our understanding of dynamic bacterial communities[26] and affords insights for bioprocessing enhancement[3–6]. However, current bioprinting routines often trade off suitability to cells for improved material manufacturability; moreover, it remains a challenge to construct macroscopic material morphologies with well-defined cell microenvironments to establish robust interactions among different cell communities.

Here, we propose a new method to address this challenge. In this work, we explore the unique applicability of cell-laden microgels at the interface of bioprinting and functional living materials. Droplet microfluidics was employed to exert control over the formation of microgels, whereby their microscopic properties could be curated to suit a range of studies and applications. Based on an aqueous two-phases system, core-shell microgels were fabricated to support the growth of both microbial communities and mammalian cellular spheroids. Furthermore, we bridge microscopically tunable building blocks with functionalities of macroscopic living materials: through a microgel dual-networking strategy, microporous PAM (Protein-based Annealed Microgel) scaffolds were constructed via extrusion bioprinting[27,28] towards bioremediation and biomanufacturing. More importantly, we demonstrated that by fabricating scaffolds with locally varying properties, i.e., a heterogeneously distributed cell population at microscale, significantly enhanced bioactivities were observed in two typical microbial consortia models. We believe our method has provided a universal strategy to construct the next generation of living materials, holding promises not only in microbial bioprocessing, but also in advanced biofabrication.

Results and discussions

From core-shell building blocks to microporous PAM scaffolds

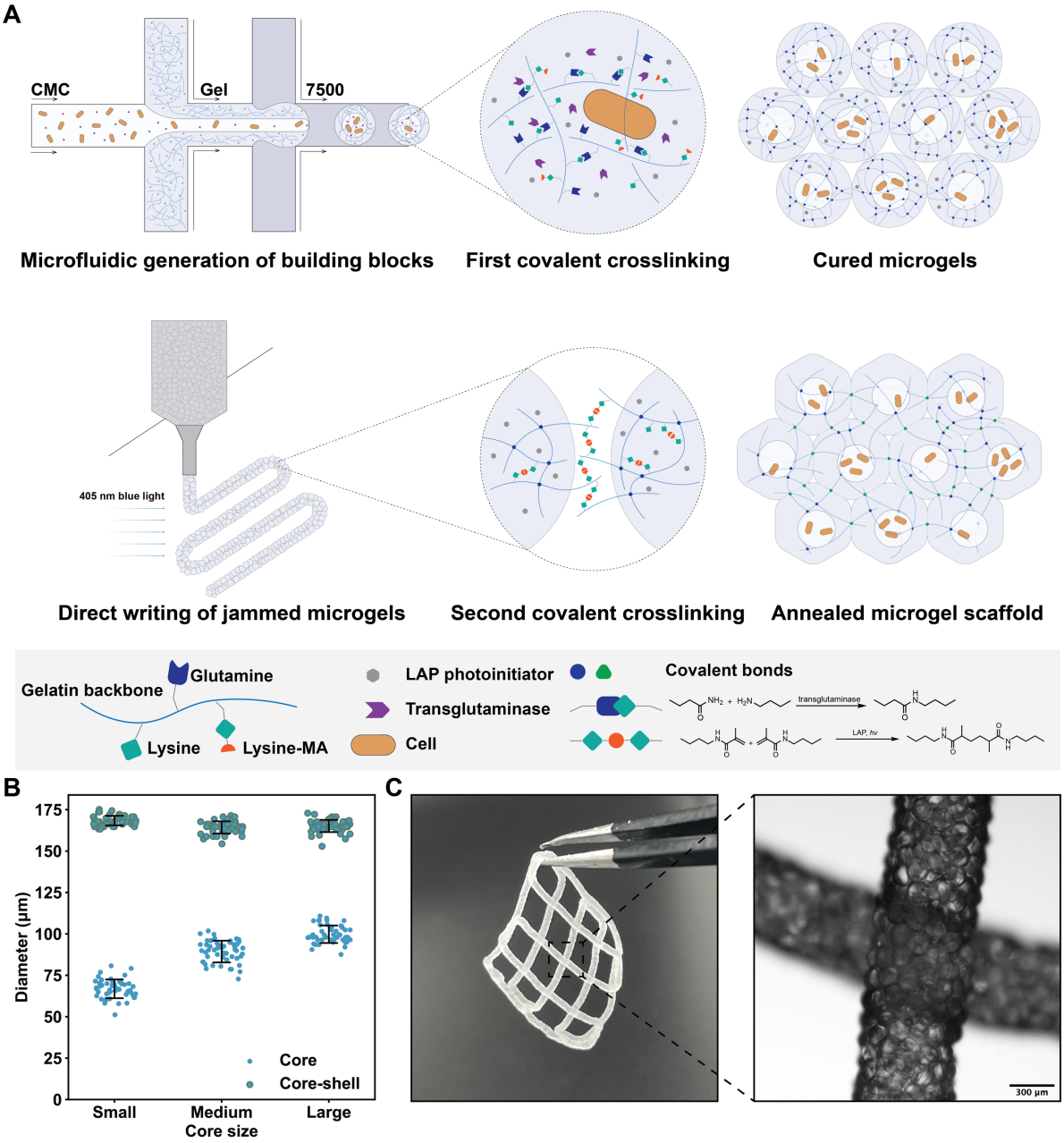

Fig. 1. Microfluidic templating of core-shell microgel building blocks for fabricating PAM scaffolds. (A) Schematic illustration of the formation of PAM scaffolds. First, the LAP-containing gelatin/gelMA polymer blend, together with cell-containing CMC solution spiked with transglutaminases, is emulsified by carrier oil into droplets within a flow-focusing microfluidic device. Droplets are then converted into microgels by enzymatic reactions, after which they are extruded and patterned into scaffolds. Finally, bule light initiates a second covalent crosslinking among jammed microgels, giving rise to PAM scaffolds. (B) By microfluidics, the core-shell ratio can be controlled. Flow rates of the hydrogel precursor solution (shell phase) and the carrier oil are controlled at 8 and 40 μL/min, respectively, and the flow rates of CMC (core phase) are 1, 2, and 3 μL/min, for small, medium, and large core size, respectively. Error bars represent standard deviation. N = 50. (C) Printed PAM scaffolds and the micrograph shows local magnification of two intersected filaments.

We started with gelatin, a collagen-derived material that has long been used in a variety of biological applications on account of its animal origin and wide availability[29], to construct living materials (Fig. 1). To afford a dual network, gelatin was first blended with its photo-crosslinkable derivative, gelMA, to generate a homogenous 15% hydrogel precursor solution spiked with 0.5% blue light photoinitiators lithium phenyl-2,4,6-trimethylbenzoylphosphinate (LAP). GelMA was synthesized according to a well-established protocol[30], with an estimated degree of functionalization of 50% by NMR (Fig. S1). The dispersed phase was emulsified in a microfluidic flow-focusing device (Fig. S2A), where a solution of 1% carboxymethylcellulose (CMC) spiked with 10 U/ml transglutaminases was flanked by hydrogel-forming solutions at the device junction, and together the dispersed phase was intersected by the carrier oil (Novec 7500 with 0.1% Pico-surf surfactant) to generate droplets (Fig. S2B). Flow rates for hydrogel precursor, CMC, and oil were respectively 8, 2, 40 μL/min, resulting in highly monodispersive core-shell droplets of ~165 μm in diameter (Coefficient of Variance, CV = 2.2%) and CMC core ~90 μm (CV = 7.4%). By microfluidics, the shell thickness could be controlled (Fig.1B and Fig. S2B), and cells could be delivered into different phases of the droplet to create heterogeneous cell distribution at microscale (Fig. S2C). Droplets were cured at room temperature overnight to allow the diffusion of transglutaminases from the CMC core into the gelatin shell which, subsequently, catalyzed the formation of isopeptide bonds between glutamine and lysine. Microgels were demulsified, followed by a direct mixing with phosphate buffered solution (PBS) containing 0.5% LAP at 4:1 volume ratio to yield a satisfactory printability. Using an extrusion 3D printer, jammed microgels could be patterned into scaffolds. Finally, 405 nm blue light initiated a second crosslinking among microgels to generate covalently stabilized PAM scaffolds mechanically stiff enough to be readily handled by a pair of tweezers (Fig. 1C). Noticeably, the dual covalent strategy is reversible, i.e., droplets can be first cured by blue light radiation and then annealed enzymatically.

SEM (Scanning Electron Microscope) images show that the dual-networked PAM scaffolds bore multiscale porosity (Fig. S3). At microgel surface there were nanopores (Fig. S3A) which are characteristic of hydrogels. Microgel packing gave rise to micropores[31], as suggested by the stretched mesh morphology of lyophilized PAM scaffolds (Fig. S3B). To further investigate how microgel size affects material properties at macroscale, we studied the degradation kinetics by trypsin of PAM scaffolds assembled from differently sized microgels (Fig. S4A), along with dual-crosslinked bulk hydrogels and non-annealed microgels. Kinetics profiles (Fig. S4B) demonstrate that the degradation of all PAM scaffolds, regardless of the microgel sizes, showed higher rates than bulk hydrogels owing to the presence of micropores that facilitated the perfusion of trypsin into the scaffolds. Moreover, the degradation tended to be slower with smaller microgel sizes due to decreased pore sizes (Fig. S4B), which could be engineered to serve as a machinery to dynamically control the diffusion profiles of molecules in/out PAM scaffolds.

Direct writing of microgel inks via extrusion printing

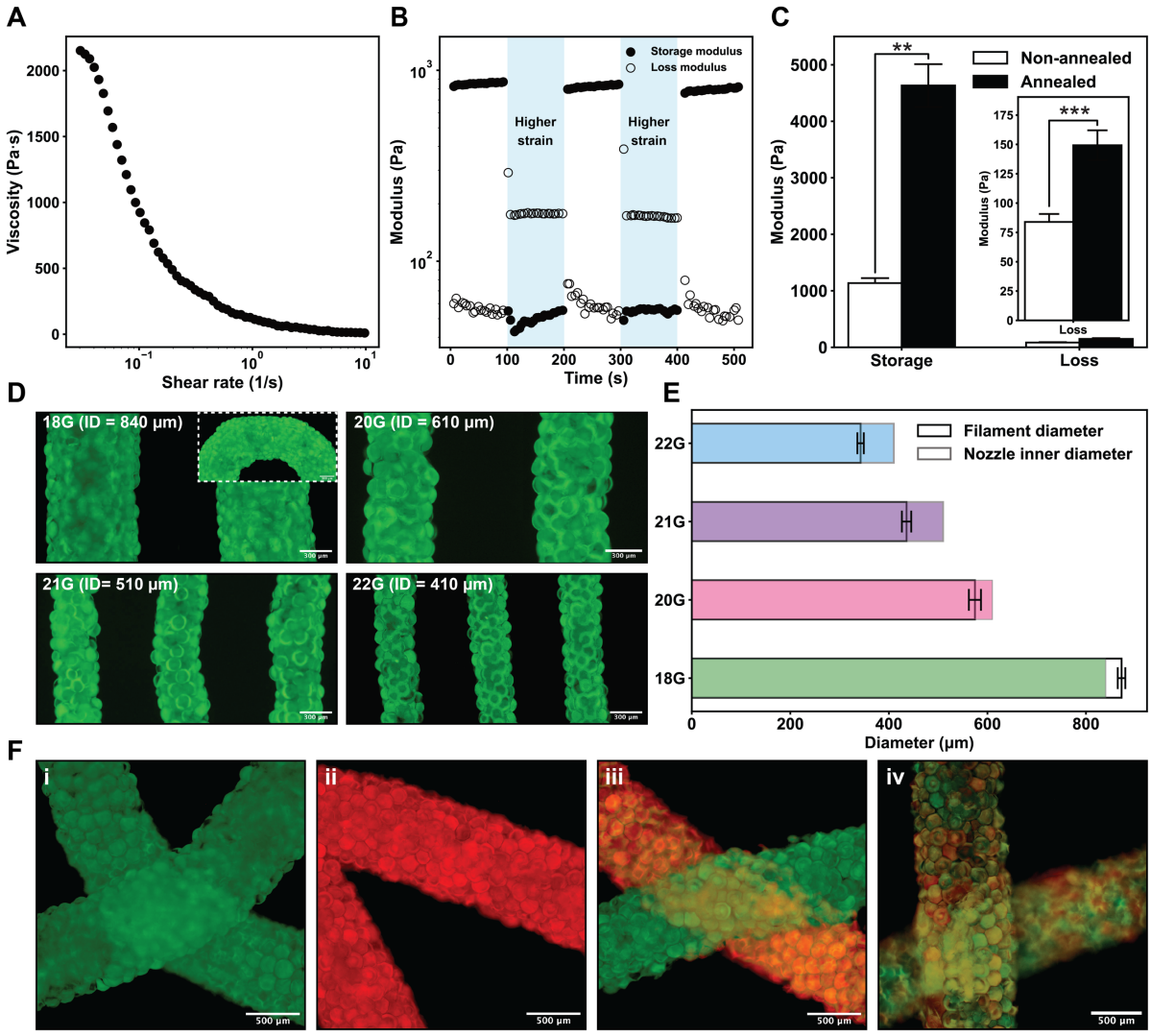

Fig. 2. Direct ink writing of jammed microgels via extrusion printing. (A)-(C) Rheology characterization of the microgel ink. Microgels are enzymatically cured. (A) Shear rate sweep experiment. Shear rate from 0 to 10 1/s. Strain 1%. (B) Step-strain sweep where low strain (1%) and high strain (90%) are cycled every 100 s. Frequency 1 Hz. (C) Storage and loss moduli before and after the photo-initiated annealing. Error bars represent standard deviation. $N = 3$. ** $p<0.01$, *** $p<0.05$, two-tailed student's t test. (D) Fluorescent images of extruded filaments printed from differently sized nozzles. Inset shows a curved corner of a filament. (E) Analysis of the filament diameters. Colored bars represent the inner diameters of the printing nozzles and the blank ones the measured diameters of printed filaments. Error bars represent standard deviation. $N = 10$. (F) Fluorescent images of scaffolds, i.e., (i) green and (ii) red homogeneous scaffolds, (iii) a macroscopically heterogenous scaffold, and (iv) a microscopically heterogenous scaffold. (D) and (F) Fluorescent microgels are generated from a mixture of gelatin with fluorophore-labeled gelMA (green: ELF-GM-GF-60, red: ELF-GM-RF-60; Yongqinquan Intelligent Equipment Co., Ltd., Suzhou, China). Multicolor fluorescent micrographs are from overlapped images.

Microgels have recently emerged as a new type of ink to fabricate 3D structures through extrusion printing[27,28,32]. In a jammed state, they can form rest structures behaving as elastic solids through physical interactions such as frictions; when sheared, the interparticle frictions are dissipated to allow the ink to flow. As such, materials that can be fashioned into microgels are theoretically printable via extrusion irrespective of their polymeric chemistry[27,28]. To quantitatively evaluate the printability of this new core-

shell microgel ink, rheology characterization was carried out first. Jammed microgels exhibited shear-thinning behavior (Fig. 2A) and could quickly recover from strain upon its removal (Fig. 2B). Collectively, this particular rheological behavior can be translated into the ability of the ink to rapidly transform from flowing liquid when sheared, to elastic solid upon leaving the nozzle. Strain sweep experiment demonstrates that the microgel ink yielded at around 30% strain (Fig. S5A); after interparticle annealing, both the storage and loss modulus increased significantly (Fig. 2C), giving rise to PAM scaffolds with enhanced mechanical strength. Moreover, the ink with a reversed dual-networking strategy shared a set of similar rheological properties (Fig. S5B-F)

We next tested the fidelity of printing. Nozzles of differing inner diameters were employed to pattern scaffolds, and the filaments all displayed uniform thickness without noticeable flattening (Fig. 2D) otherwise affected by surface tension upon contacting with the solid surface. Consequently, the filament diameters were faithful to printing nozzles and even slightly smaller using 20G, 21G, and 22G nozzles (Fig. 2E) owing to increased edge jaggedness. We then tested the compatibility of the microgel ink with a commercial extrusion 3D printer (Fig. S6). Microgel ink with optimized printability was loaded into a dispersion cartridge coupled with a three-axis mechanical robotic arm (EFL-BP-6601, Yongqinquan Intelligent Equipment Co., Ltd., Suzhou, China). The extrusion and the writing speed of the microgel ink were controlled pneumatically and by the robotic arm, respectively. Unlike continuous material-based extrusion printing where the filament thickness can be controlled by both the extrusion and the writing speed due to filament fusion[33], we found that the thickness of the printed microgel ink is barely dependent on neither speed but the size of the nozzle. Thus, mismatched speeds will lead to either filament breaking (extrusion<writing) or undesired filament buildup (extrusion>writing, Fig. S7). As a result, by matching the speed of ink extrusion and writing, we were able to pattern the microgel ink into various predefined shapes (Fig. S6A) and multilayered structures (Fig. S6B and Fig S15A). Besides homogenous structures (Fig. 2F, i and ii), heterogenous structures across different scales (Fig. 2F, iii and iv) could also be fabricated.

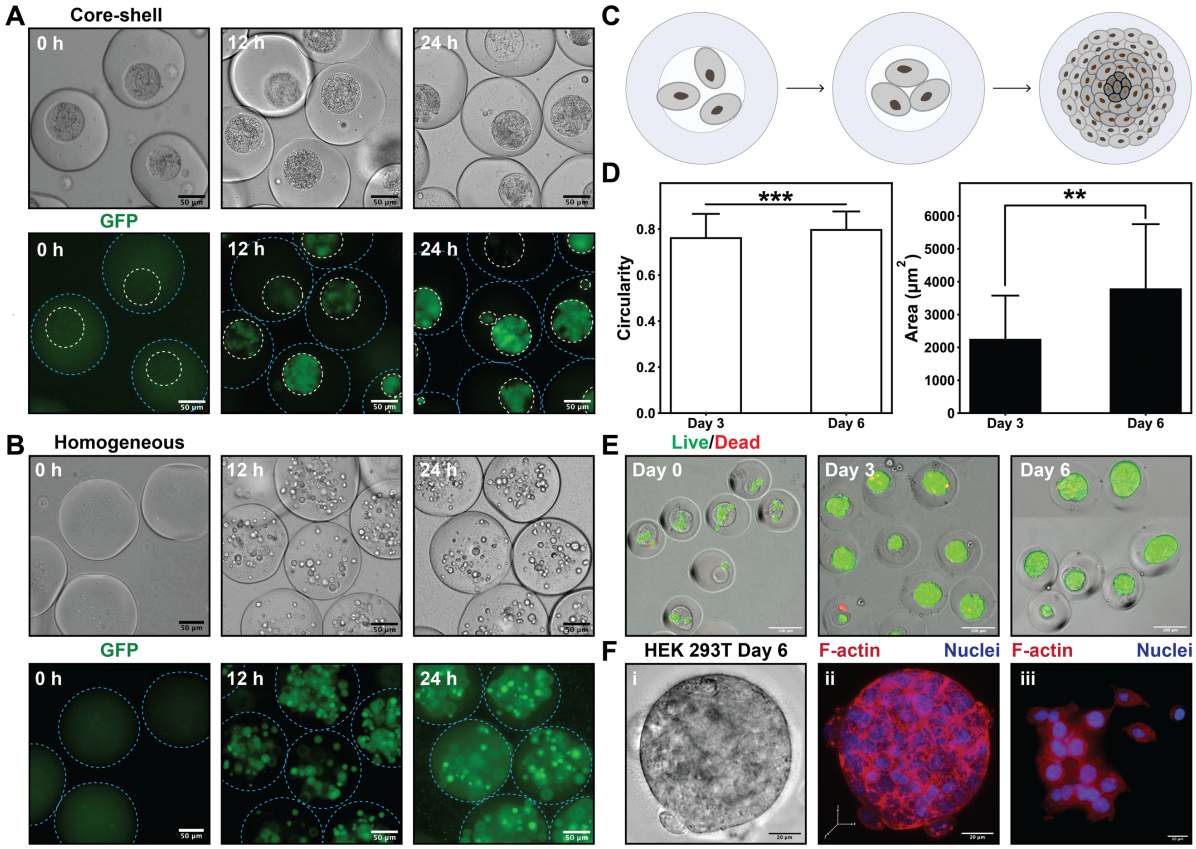

Fig. 3. Core-shell microgels for cell culture. Left panel: GFP *Escherichia Coli* (*E. coli.*) in core-shell and homogeneous microgels. Right panel: formation and characterization of HEK 293T cellular spheroids in core-shell microgels. (A) Proliferation of GFP *E. coli.* in the core-shell microgels. Cell growth is confined inside the aqueous microgel cores. (B) Proliferation of *E. coli.* in the homogenous microgels. *E. coli* proliferate locally to form visible microcolonies. Blue and white dashed lines outline the microgels and the CMC cores, respectively. (C) Schematic representation of the formation of multicellular spheroids. Due to the spatial confinement, cells are allowed to interact in all three dimensions to form multicellular spheroids featuring a hierarchical structure. Drawing is not to scale. (D) Growth of HEK 293T spheroids from day 3 to day 6, quantified by spheroid circularity and area. Error bars represent standard deviation. N = 100. ** $p<0.0001$, *** $p<0.01$, two-tailed student's t test. (E) Live/Dead staining of cell-laden microgels at day 0, day 3, and day 6. Live cells (green) and dead cells (red) are stained with calcein acetoxymethyl (calcein AM) and ethidium homodimer-1 (EthD-1), respectively. Scale bars are 100 μm. (F) Cytoskeletal structure of HEK 293T spheroids. (i) Brightfield image of a HEK 293T spheroid and (ii) its confocal microscopic image. (iii) Cytoskeletal structure of HEK 293T from monolayer culture. F-actin and nuclei are stained with phalloidin and 4', 6-diamidino-2-phenylindole (DAPI), respectively. Confocal fluorescent micrograph is rendered from cross-sectional images at different vertical positions (Fig. S12). Scale bars are 20 μm.

We next investigated the proliferation of cells in the core-shell building blocks (Fig. 3). We set out to compare how microorganisms such as bacteria grew in core-shell microgels with homogenous microgels. *E. coli* were allowed to grow in cured microgels for 24 hours. In core-shell microgels, to a great extent, cell growth was physically confined, which led to a concentrated bacterial community in the aqueous core (Fig. 3A). In stark contrast, bacteria in homogeneous microgels proliferated locally and formed sporadic microcolonies (Fig. 3B). We also discovered that such spatial confinement could restrain bacteria from escaping to the environment more effectively (Fig. S8A), in accordance with

measurements of GFP absorption from media (Fig. S8B). As cell leakage constitutes a major challenge in the field of living materials[34], especially when genetically modified microorganisms are involved, the use of core-shell microgels might offer strategies into solutions to this problem[35]. Furthermore, microbes could proliferate in the PAM scaffolds in a similar fashion without notable cross contamination among adjacent microgels (Fig. S9).

Applicability of core-shell microgels for mammalian cell culture was also characterized (Fig. 3C-3F). The delivery of cells into the microgels followed Poisson distributions (Fig. S10). Likewise, cells were spatially confined and allowed to proliferate and interact in all dimensions inside microgels and to self-assemble into high cell density spheroids (Fig. 3C). Human Embryonic Kidney (HEK) 293T cells developed into cellular spheroids after three days in microgels (Fig. 3E) and displayed a high circularity (Fig. 3D). From day 3 to day 6, the spheroids size increased 80% (Fig. 3D) and maintained high viability, as evidenced by Live/Dead staining (Fig. 3E). Moreover, we observed that within some spheroids resided a population of dead cells (Fig. S11), presumably the necrotic cores frequently reported in tumor spheroids models, owing to the hindered diffusion of oxygen and nutrients into the deeper regions of spheroids[36]. The cytoskeleton of HEK 293T spheroids was composed of densely packed nuclei surrounded by a meshwork of cortical actin (Fig. 3F, ii), epitomizing the predominance of cell-cell interactions, in contrast to monolayer-based cell culture, where actin was organized into cytoplasmic fibers (Fig. 3F, iii). To conclude, HEK 293T are able to form well-structured cellular spheroids inside core-shell microgels with high cell viability, indicating their suitability for future applications such as 3D cell culture and biofabrication.

Microscopic segregation enhances bioactivities of immobilized microbial consortia

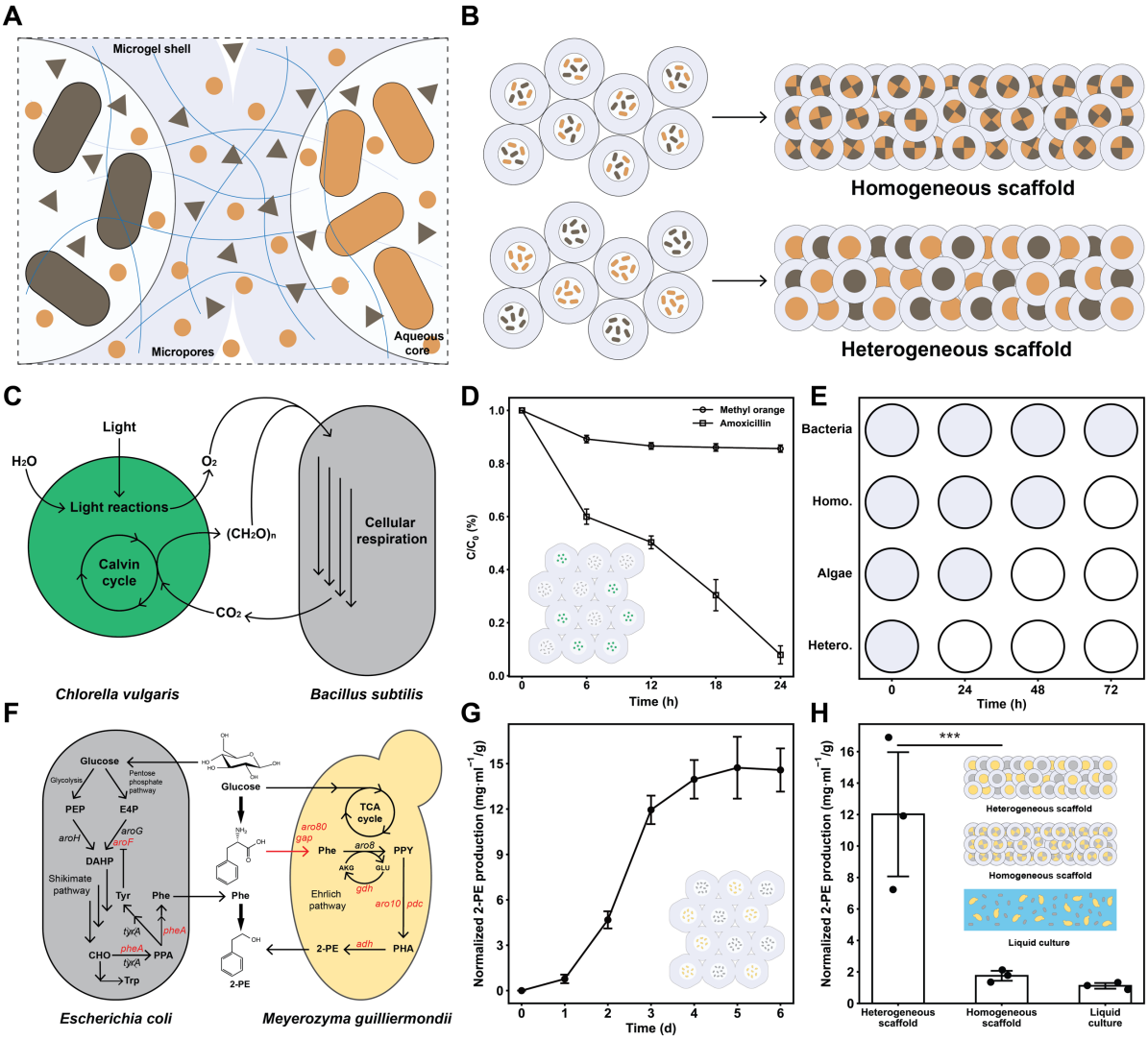

Fig. 4. Miscroscopic compartmentalziation enhances bioactivities of microbial consortia. (A) PAM scaffolds immobolize and segregate microbial consortia at microscopic space, which prevents competetive growth while enabling a more efficient mass transfer of metabolites between speceis. (B) Cell-laden core-shell microgels are jammed and printed into scaffolds. Heterogeneous and homogeneous scaffolds are defined as: a mixed population of microgels containing two different microorganism species, respectively, and a homogeneous population of microgels containing a mixture of two microorganisms. (C)-(E) Mutualism model of microbial consortia. (C) Schematic representation of the natural symbiotic relationship between *Chlorella vulgaris* and *Bacillus subtilis*. (D) Removal of methyl orange (100 mg/L) and amoxicillin (300 mg/L) in synthetic wastewater by heterogeneous PAM scaffolds in 24 hours. Error bars represent standard deviation. N = 3. (E) Characterization of scaffold disintegration in 72 hours. Solid circle marks an unbroken scaffold whereas hollow circle scaffold markedly disintegrating. For all experiments, scaffolds are subjected to a cyclic 12:12 hour of light/darkness condition and incubated at 25 °C. (F)-(H) Competitive growth model of microbial consortia. (F) The synthetic microbial consortium of genetically engineered *Escherichia Coli* and *Meyerozyma guilliermondii* for producing 2-PE from glucose. Overexpressed genes are marked red. Crossed gene *tyrA* is knocked out by CRISPR. (G) The production of 2-PE from heterogeneous scaffolds over 6 days, which is normalized by respective scaffold weights. Error bars represent standard deviation, N = 3. (H) Comparison of bioprocessing in terms of normalized 2-PE production over 3 days. Error bars represent standard deviation, N = 3. *** $p<0.05$, two-tailed student's t test. For both scaffolds, the production is normalized by corresponding scaffold weights; for liquid culture, CMC containing consortia is directly

inoculated into media, the cell loading of which is the same as the scaffolds, and 2-PE production is normalized to imaginary scaffolds weights of heterogeneous and homogeneous combined.

Through interconnected core-shell microgels, PAM scaffolds possess not only controllable porosity but also the capability to segregate multi-species communities at microscale (Fig. 4A), which together effects a more efficient transfer of nutrients and metabolites between the scaffold and environment as well as interacting species while precluding their competitive growth[6]. We then examined whether this method could enhance bioactivities of immobilized microbial consortia through a spatial division of labor (Fig. 4B) compared to direct mixing of consortia. First, we studied a microalgae-bacteria system consisting of photoautotrophic *Chlorella vulgaris* and aerobic *Bacillus subtilis* (Fig. 4C) for its capacity to bioremediate organic contaminants[37]. This microbial consortium is a naturally occurring symbiosis where the microalgae fix carbon dioxide emitted from the bacteria into carbon sources whilst producing oxygen through photosynthesis for bacteria to respirate (Fig. 4C). Heterogeneous PAM scaffolds immobilizing the consortium (Fig. 4D inset) were fabricated and submerged in synthetic wastewater containing methyl orange or amoxicillin. Over 90% of amoxicillin (300 mg/L) was removed in 24 hours and around 15% for methyl orange (100 mg/L). However, we also observed that after 48 hours, scaffolds were all degraded and liquified (Fig. S13A), which could be ascribed to hydrolysis of scaffolds by microbial proteases. We sought to utilize this phenomenon as a qualitative measure of microbial bioactivity of the consortium (Fig. 4E). Four 3x3 lattice-shaped PAM scaffolds were fabricated and immersed in BG11 media that respectively encapsulated: microbial consortium in separate microgels (heterogeneous) and in single microgels (homogeneous), microalgae, and bacteria (Fig. 4E and Fig. S13B). While the scaffold immobilizing microalgae began to decompose after 24 hours, for 72 hours, the scaffold with bacteria largely retained its structure, as the nutrient-deficient medium is unfavorable for the growth of *Bacillus subtilis*. Within 24 hours, the heterogenous scaffold started disintegrating into smaller fragments whereas the homogenous scaffold maintained structural integrity until day 3. In conclusion, in BG11 media, *Chlorella vulgaris* are able to digest the PAM scaffolds; moreover, the presence of *Bacillus subtilis* in separate microgels expedites the degradation process, suggestive of an improved bioactivity compared with microalgae alone, even though the latter had twice the microalgae load. Also, co-encapsulation of the microalgae-bacteria consortium in single microgels attenuates the bioprocess, as the heterogeneous scaffold exhibits a better efficiency in digesting scaffolds in spite of an equivalent cell load to the homogeneous scaffold.

Finally, we tested a synthetic fungi-bacteria consortium to ferment glucose into 2-phenylethanol (2-PE) (Fig. 4F). In this enzymatic cascade (Fig. 4F and Fig. S14), the carbon source is first converted by *Escherichia Coli* into the intermediate l-phenylalanine that is further metabolized into 2-PE by *Meyerozyma guilliermondii,* a species of yeast that is reported to produce and tolerate a high concentration of 2-PE[38]. In light of the intimate connection between the biosynthesis pathway of l-phenylalanine and that of the other aromatic amino acids, especially l-tyrosine, the *pheA* gene, encoding the key enzyme for the biosynthesis of l-phenylalanine, is overexpressed while *the tyrA* gene is knocked out by CRISPR, in order to preferentially channel the precursor chorismic acid (CHO) into l-phenylalanine. Additionally, the expression of *aroF*, an essential gene in the shikimate pathway and sensitive to l-tyrosine, is also

enhanced. To promote the conversion of l-phenylalanine to 2-PE, genetic modifications are conducted to strengthen the intrinsic Ehrlich pathway of *Meyerozyma guilliermondii*, which comprises three steps: first, l-phenylalanine is transaminated to phenylpyruvate (PPY) with α-ketoglutaric acid (AKG), generating byproduct glutamate (GLU). Accordingly, non-pathway-specific glutamate dehydrogenases (encoded by *the gdh* gene) are overexpressed to increase the supply of AKG. Subsequently, PPY is converted to phenylacetaldehyde (PHA) and further reduced to 2-PE, where key enzymes such as phenylpyruvate decarboxylases (*aro10* and *pdc*) and alcohol dehydrogenases (*adh*) are overexpressed to facilitate the conversion. Besides these genes, *gap*, the general amino acid permeases, and *aro80* that activates the transcription of aromatic amino acid catabolic genes, are also overexpressed to increase the efficiency of bioconversion.

As both microorganisms utilize glucose as the carbon source, they form a competitive relationship. We first measured the kinetics of 2-PE production from heterogeneous scaffolds. A mixed population of microgels respectively encapsulated *Escherichia Coli* or *Meyerozyma guilliermondii* were fabricated into 5-layered 3x3 lattice scaffolds and incubated in synthetic culture media to ferment glucose into 2-PE (Fig. S15). Result displays (Fig. 4G) sigmoidal kinetics that peaked at around day 2 and gradually leveled off after 3 days of fermentation. The endpoint production was 14.23±1.12 $mg \cdot mL^{-1}/g$ (hydrogel), among the highest in literature (non-normalized production 6.21±0.73 mg/mL). Next, we compared the yield of 2-PE between two different sets of scaffolds (Fig. 4H). Remarkably, the heterogeneous scaffolds generated over 6-fold higher 2-PE than homogenous scaffolds did in 3 days. We also found the homogeneous scaffolds produced more 2-PE in comparison with liquid culture (Fig. 4H), which was possibly attributed to the closer physical contact of two microorganisms brought by growth confinement in microgels. At last, we examined the reusability of scaffolds for 2-PE batch production (Fig. S15). Scaffolds could maintain integrity during the first batch (3 days); despite gradual structural collapse henceforth, scaffolds were not fully compromised after 4 batch processes in a row (12 days in total). However, the production of 2-PE significantly reduced (Fig. S15G), especially for heterogeneous scaffolds, which decreased by 70% at the second batch whereas 20% for homogeneous scaffolds. 2-PE production for both scaffolds deteriorated batch by batch and almost completely stopped after the third batch; nevertheless, the heterogeneous scaffolds still yielded more 2-PE (Fig. S15G). The declining performance of scaffolds could be caused by cells' escaping and reattaching to the inner surface of the scaffold that upset the growth balance of two microbial species, as they could not be entirely scoured away by fresh media between batches.

Conclusion

Together, the work presented here describes a new approach for constructing living materials via a common extrusion bioprinting routine. Through a microgel dual-networking method, covalently stabilized macroscopic functional living materials can be printed and readily deployed for bioremediation and biomanufacturing. We used core-shell microgel to spatially organize the cell communities, from which a heterogeneous distribution of cells can be established to promote the inter-species communications of microbial consortia amid the generation of programmable morphologies by extrusion printing. As a result, our results demonstrate remarkably improved bioactivities from two different microbial symbiotic relationships. Although the protein-based material might not be the most ideal choice for microbial applications due to its susceptibility to protease hydrolysis, we envisage future efforts of using more stable materials for such applications. Still, we believe our proposed method represents a new paradigm to construct functional living materials for microbial bioprocessing and also holds potentials towards advanced biofabrication[39].

Acknowledgements

National Key Research and Development Program of China (2021YFC2104300), the National Natural Science Foundation of China (21901117, 32111530117) and State Key Laboratory of Materials-Oriented Chemical Engineering (KL20-02) to Z.Y. The Newman Foundation, the Wellcome Trust, the European Research Council under the European Union's Seventh Framework Programme (FP7/2007-2013) through the ERC Grant PhysProt (Agreement No. 337969) to T.P.J.K. Cancer Research UK (CRUK) Cambridge Institute Core Grant (C9545/A29590) to M.N.; CRUK Early Detection Pump Priming awards (C20/A20976) to T.K. and M.N. Chinese Scholarship Council (H.Z.)

Author contributions

Y.O., T.P.J.K., and Z.Y. conceived and designed the experiments. Y.O. performed all experiments, analyzed data, and wrote the manuscript. S.C., H.Z., C.G., and Y.Z. performed experiments. W.Y. and F.X. provided the genetically engineered microorganisms. M.N. provided mammalian cell lines and tissue culture facility. T.K. and Z.Y. supervised the project and revised the manuscript. All authors reviewed the paper.

Conflict of interest

The authors declare no conflicts of interest.

References

1. Rodrigo-Navarro, A., Sankaran, S., Dalby, M. J., del Campo, A. & Salmeron-Sanchez, M. Engineered living biomaterials. *Nat. Rev. Mater.* **6**, 1175–1190 (2021).
2. Shang, L., Shao, C., Chi, J. & Zhao, Y. Living Materials for Life Healthcare. *Accounts Mater. Res.* **2**, 59–70 (2021).
3. He, F. *et al.* 3D Printed Biocatalytic Living Materials with Dual-Network Reinforced Bioinks. *Small* **18**, 1–9 (2022).
4. Qian, F. *et al.* Direct Writing of Tunable Living Inks for Bioprocess Intensification. *Nano Lett.* **19**, 5829–5835 (2019).
5. Saha, A. *et al.* Additive Manufacturing of Catalytically Active Living Materials. *ACS Appl. Mater. Interfaces* **10**, 13373–13380 (2018).
6. Johnston, T. G. *et al.* Compartmentalized microbes and co-cultures in hydrogels for on-demand bioproduction and preservation. *Nat. Commun.* **11**, 1–11 (2020).
7. Schaffner, M., Rühs, P. A., Coulter, F., Kilcher, S. & Studart, A. R. 3D printing of bacteria into functional complex materials. *Sci. Adv.* **3**, (2017).
8. Lutolf, M. P. & Hubbell, J. A. Synthetic biomaterials as instructive extracellular microenvironments for morphogenesis in tissue engineering. *Nat. Biotechnol.* **23**, 47–55 (2005).
9. Chrisnandy, A., Blondel, D., Rezakhani, S., Broguiere, N. & Lutolf, M. P. Synthetic dynamic hydrogels promote degradation-independent in vitro organogenesis. *Nat. Mater.* (2021) doi:10.1038/s41563-021-01136-7.
10. Gjorevski, N. *et al.* Tissue geometry drives deterministic organoid patterning. *Science (80-.).* **375**, (2022).
11. Duraj-Thatte, A. M. *et al.* Programmable microbial ink for 3D printing of living materials produced from genetically engineered protein nanofibers. *Nat. Commun.* **12**, (2021).
12. Huang, J. *et al.* Programmable and printable Bacillus subtilis biofilms as engineered living materials. *Nat. Chem. Biol.* **15**, 34–41 (2019).
13. Wang, Y. *et al.* Living materials fabricated via gradient mineralization of light-inducible biofilms. *Nat. Chem. Biol.* **17**, 351–359 (2021).
14. Li, Y. *et al.* Patterned Amyloid Materials Integrating Robustness and Genetically Programmable Functionality. *Nano Lett.* **19**, 8399–8408 (2019).
15. Tang, T. C. *et al.* Materials design by synthetic biology. *Nat. Rev. Mater.* **6**, 332–350 (2021).
16. Baker, B. M. & Chen, C. S. Deconstructing the third dimension-how 3D culture microenvironments alter cellular cues. *Journal of Cell Science* vol. 125 3015–3024 (2012).

17. Mao, A. S. *et al.* Deterministic encapsulation of single cells in thin tunable microgels for niche modelling and therapeutic delivery. *Nat. Mater.* **16**, 236–243 (2017).
18. Zhao, X. *et al.* Injectable Stem Cell-Laden Photocrosslinkable Microspheres Fabricated Using Microfluidics for Rapid Generation of Osteogenic Tissue Constructs. *Adv. Funct. Mater.* **26**, 2809–2819 (2016).
19. Griffin, D. R., Weaver, W. M., Scumpia, P. O., Di Carlo, D. & Segura, T. Accelerated wound healing by injectable microporous gel scaffolds assembled from annealed building blocks. *Nat. Mater.* **14**, 737–744 (2015).
20. Daly, A. C., Prendergast, M. E., Hughes, A. J. & Burdick, J. A. Bioprinting for the Biologist. *Cell* **184**, 18–32 (2021).
21. Zhang, Y. S. *et al.* 3D extrusion bioprinting. *Nat. Rev. Methods Prim.* **1**, (2021).
22. Daly, A. C., Davidson, M. D. & Burdick, J. A. 3D bioprinting of high cell-density heterogeneous tissue models through spheroid fusion within self-healing hydrogels. *Nat. Commun.* **12**, 1–13 (2021).
23. Skylar-Scott, M. A. *et al.* Biomanufacturing of organ-specific tissues with high cellular density and embedded vascular channels. *Sci. Adv.* **5**, (2019).
24. Brassard, J. A., Nikolaev, M., Hübscher, T., Hofer, M. & Lutolf, M. P. Recapitulating macro-scale tissue self-organization through organoid bioprinting. *Nat. Mater.* **20**, 22–29 (2021).
25. Liu, Y. *et al.* Bio-assembling Macro-Scale, Lumenized Airway Tubes of Defined Shape via Multi-Organoid Patterning and Fusion. *Adv. Sci.* **8**, 1–11 (2021).
26. Krishna Kumar, R. *et al.* Droplet printing reveals the importance of micron-scale structure for bacterial ecology. *Nat. Commun.* **12**, 1–12 (2021).
27. Highley, C. B., Song, K. H., Daly, A. C. & Burdick, J. A. Jammed Microgel Inks for 3D Printing Applications. *Adv. Sci.* **6**, (2019).
28. Xin, S. *et al.* Generalizing hydrogel microparticles into a new class of bioinks for extrusion bioprinting. *Sci. Adv.* **7**, 1–12 (2021).
29. Xu, Y. *et al.* Microfluidic Templating of Spatially Inhomogeneous Protein Microgels. *Small* **2000432**, 1–9 (2020).
30. Loessner, D. *et al.* Functionalization, preparation and use of cell-laden gelatin methacryloyl-based hydrogels as modular tissue culture platforms. *Nat. Protoc.* **11**, 727–746 (2016).
31. Daly, A. C., Riley, L., Segura, T. & Burdick, J. A. Hydrogel microparticles for biomedical applications. *Nat. Rev. Mater.* (2019) doi:10.1038/s41578-019-0148-6.
32. Daly, A. C., Riley, L., Segura, T. & Burdick, J. A. Hydrogel microparticles for biomedical applications. *Nat. Rev. Mater.* **5**, 20–43 (2020).
33. He, Y. *et al.* Research on the printability of hydrogels in 3D bioprinting. *Sci. Rep.* **6**, 1–

13 (2016).

34. Zhao, S. *et al.* A new design for living cell-based biosensors: Microgels with a selectively permeable shell that can harbor bacterial species. *Sensors Actuators, B Chem.* **334**, 129648 (2021).
35. Tang, T. C. *et al.* Hydrogel-based biocontainment of bacteria for continuous sensing and computation. *Nat. Chem. Biol.* **17**, 724–731 (2021).
36. Hirschhaeuser, F. *et al.* Multicellular tumor spheroids: An underestimated tool is catching up again. *J. Biotechnol.* **148**, 3–15 (2010).
37. Gonçalves, A. L., Pires, J. C. M. & Simões, M. A review on the use of microalgal consortia for wastewater treatment. *Algal Res.* **24**, 403–415 (2017).
38. Yan, W. *et al.* The draft genome sequence of Meyerozyma guilliermondii strain YLG18, a yeast capable of producing and tolerating high concentration of 2-phenylethanol. *3 Biotech* **9**, 1–5 (2019).
39. Kim, S. jeong, Kim, E. M., Yamamoto, M., Park, H. & Shin, H. Engineering Multi-Cellular Spheroids for Tissue Engineering and Regenerative Medicine. *Adv. Healthc. Mater.* **9**, 1–18 (2020).